Implementation of Frequency Adaptive Damped SOGI Based Control for Power Quality Improvement in Wind-Solar-BES Based AC Microgrids

[1]Shadab Murshid, *Member*, *IEEE*, [1]Bhim Singh, *Fellow*, *IEEE*, [2]H. B. Gooi, *Life Senior Member, IEEE* and [2]Y. S. Eddy Foo, *Member, IEEE*
[1]Department of Electrical Engineering, Indian Institute of Technology Delhi, New Delhi -110016, India
(Email: mail2smurshid@gmail.com and bsingh@ee.iitd.ac.in)
[2]School of Electrical and Electronic Engineering, Nanyang Technological University, Singapore 639798.
(Email: ehbgooi@ntu.edu.sg and eddyfoo@ntu.edu.sg)

***Abstract*—This work presents a frequency adaptive damped second order generalized integrator (FA-DSOGI) for power quality (PQ) improvement in AC microgrids. The presented microgrid comprises a wind and solar photo-voltaic (PV) based energy generation, which is coupled to the single-phase AC grid. A non-linear local load is coupled at the point of common coupling (PCC) with the grid. A battery energy storage (BES) is also connected to the DC link through a bidirectional converter (BDC) which can support the local load when the grid is not available. A hill climbing based maximum power point tracking (MPPT) technique is utilized for optimum power extraction from both wind and solar PV based energy sources. A back electromotive force (BEMF) based sensor-less field oriented control (FOC) technique is utilized for controlling the speed of permanent magnet synchronous generator (PMSG) based wind generator. The FA-DSOGI based control technique is utilized for extracting the fundamental load component from the distorted load current and the generation of switching pulses for the VSC. The performance of the presented system is confirmed using the developed laboratory prototype.**

***Index Terms*—Frequency Adaptive Control, Damped SOGI, AC Microgrid, Wind Power Generation, Solar Power Generation**

I. INTRODUCTION

The electrical energy has evolved as a vital necessity for the human beings. With increasing industrialization, the demand for electrical energy is further increasing. Conventionally, fossil fuel based energy sources have been utilized for electricity generation, however, their increased usage has resulted in global warming [1]. The burning of conventional energy sources also emits harmful flue gases, which would adversely affect the living beings. The utilization of renewable energy sources presents an appropriate solution to mitigate the aforementioned challenges. Owing to their efficient utilization and economic viability, wind and solar photo-voltaic (PV) based power generation systems are receiving greater attention in recent days. However, the intermittency associated with these sources, poses serious challenges to the grid stability. In such a scenario, the integration of multiple distributed energy sources, improves the system reliability.

Wind energy generation systems (WEGS) require a generator for electricity generation. Owing to the higher efficiency, smaller size and lighter weight, the permanent magnet synchronous generator (PMSG) is widely used as the electric generator among a wide variety of electric generators [2]. However, for the WEGS application, the PMSG speed also needs to be varied continuously under varying wind speed for the optimum power extraction. As the field oriented control (FOC) technique provides an excellent speed control, the same has been utilized here for energy generation using WEGS. The FOC technique requires the speed and position information for their implementation. An encoder is generally utilized for this purpose, however, as its use reduces the reliability and increases the cost, the speed and position information needs to be estimated [3]. Due to the simplicity of implementation and better performance under medium and high speed operation, a back EMF based technique is utilized in this work for speed and position estimation.

A maximum power tracking technique (MPPT) is required for the optimum power extraction from the wind and solar based energy sources. A number of MPPT techniques are present in the existing literature for this purpose. A hill climbing based MPPT technique varies the control variable in the direction of peak power and is widely used due to their ease and effectiveness of implementation [4]. As for WEGS, the output power varies with generator speed and for solar PV generation, the output power varies with solar PV array voltage, the hill climbing technique generates the reference generator speed and reference solar PV voltage, which need to be controlled for optimum power generation. Although the use of MPPT extracts the optimum power, the intermittency is still associated due to uneven power generation from these sources [5]. In order to meet this issue, battery energy storage (BES) is introduced at the DC link using bidirectional converter (BDC). The power flow from the battery is regulated such that the battery would feed the power during energy deficit condition and would absorb when excess power is available. The BES can also support the local load when the grid is not available.

For grid connected systems, the power quality (PQ) has always remained an important parameter [6]. However, the increase in non-linear loads and power electronic equipment, seriously affect the PQ. Such equipment pollute the AC grid and affect the performance of sensitive equipment coupled to the same point of common coupling (PCC). Therefore, an effective control scheme is required for controlling the grid side converter (GSC), which feed the active power into the grid. The control scheme also performs the function of PQ improvement by maintaining unity power factor and minimizing the current total harmonic distortion (THD).

Synchronous reference frame theory and instantaneous reactive power control theory have been used in the past for this purpose, however, they utilize multiple frame

transformations [7]. Some of the signal processing techniques are being utilized nowadays for PQ improvement. Recently, the delayed signal cancellation (DSC) technique utilizing multiple DSCs has been presented in [8]. The presented method provides an excellent performance, however, the use of multiple DSCs increases the computation burden and, therefore, require high end processor for their implementation. A least mean fourth (LMF) based technique for PQ improvement in a grid interface system is presented in [9]. Owing to the fourth order optimization, this method provides a good dynamic performance, however, it exhibits a poor steady-state performance and DC offset elimination ability. A second order generalized integrator (SOGI) is also being used for fundamental load current component extraction [10]. The SOGI provides two orthogonal components i.e. in-phase component which acts a band pass filter and quadrature component which acts as a low pass filter (LPF). As the quadrature component acts as a LPF, it is unable to reject the DC offset. The answer to this issue lies in the use of two cascaded SOGIs, however, this increases the computational burden and also introduces transition delay [11]. A damped SOGI based control structure with the capability of faster convergence, good noise and DC offset rejection capability and improved steady state response is presented in [12]. However, the presented damped SOGI is unable to perform under frequency variation. Therefore, a frequency adaptive damped SOGI (FA-DSOGI) is proposed in this work for PQ improvement in the presented system. The presented wind-solar-BES based AC microgrid utilizing FA-DSOGI based control structure is developed in the laboratory. It has been realized from the experimental results that this system meets the IEEE-519 standard [6].

II. System Configuration and Control

Fig. 1 shows the configuration for the presented microgrid. The presented system comprises a PMSG based WEGS, a solar PV based energy generation, BES connected to the DC bus using BDC and single phase AC grid connected to the DC bus through the grid side converter (GSC). A BEMF based sensor-less FOC method is applied for the speed control of WEGS. The solar PV array is directly coupled to the DC bus and form a single stage topology which improves the system efficiency by eliminating the intermediate stage converter. The DC link voltage is varied such that peak power is harnessed from solar PV array. A hill climbing algorithm is employed for peak power extraction from the WEGS and solar PV array. A FA-DSOGI based control is utilized for improving the PQ through controlling the GSC. The BDC converter is controlled through the hysteresis controller. An elaborated discussion on the employed control techniques is presented as follows.

A. MPPT

A hill climbing based MPPT technique, which varies the control variable in the direction of maximum power, is utilized here for the optimum power extraction. The governing equations for the hill climbing MPPT technique are expressed as follows.

$$CV_{ref}(n) = CV_{ref}(n\text{-}1) + \Delta Step;\ \text{if} \begin{Bmatrix} \Delta P > 0 \text{ and } \Delta CV > 0 \\ \Delta P < 0 \text{ and } \Delta CV < 0 \end{Bmatrix} \quad (1)$$

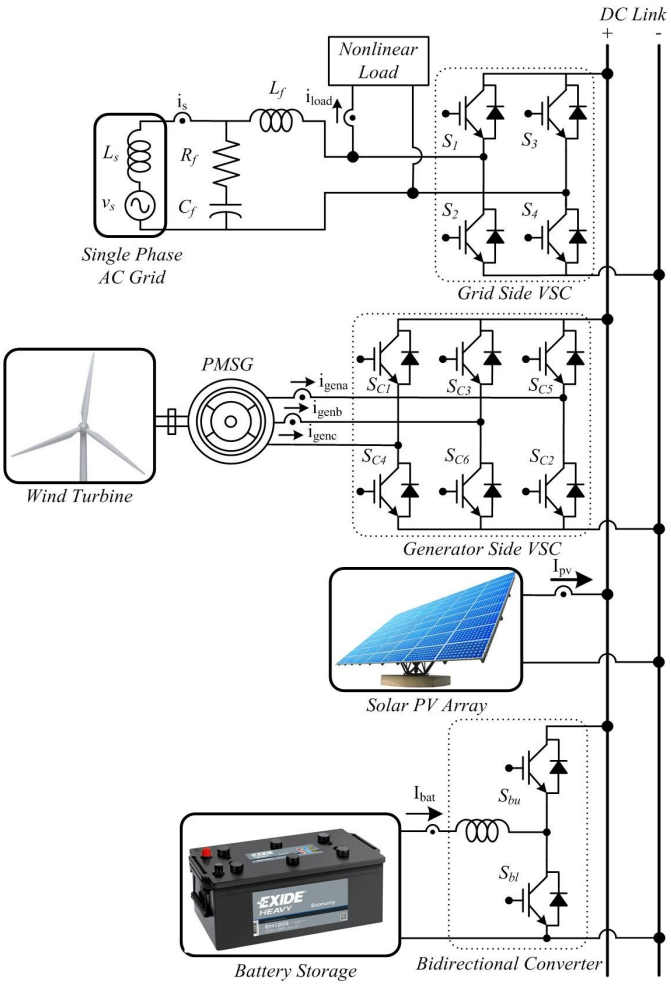

Fig. 1. Single phase grid integrated Wind-PV-BES based microgrid

$$CV_{ref}(n) = CV_{ref}(n\text{-}1) - \Delta Step;\ \text{if} \begin{Bmatrix} \Delta P > 0 \text{ and } \Delta CV < 0 \\ \Delta P < 0 \text{ and } \Delta CV > 0 \end{Bmatrix} \quad (2)$$

where, CV_{ref} is the reference control variable; ΔCV is the change in control variable and P is the power and ΔP is the change in power. The control variable for WEGS is the reference generator speed (ω_{gref}), whereas, the control variable for solar PV generation is the PV array voltage (V_{pvref}).

B. Control of WEGS

The control of WEGS comprises rotor speed and position estimation and speed control of the PMSG as shown in Fig.2.

1) Estimation of Rotor Speed and Position

A BEMF method is utilized for estimating the PMSG speed and position.

Stator voltages in αβ0 frame (v_α and v_β) are estimated using the DC link voltage (V_{dc}) and switching pulses using (S_{C1}, S_{C3}, S_{C5}) as,

$$v_\alpha = \frac{V_{dc}}{3}\left(2S_{C1}\text{-}S_{C3}\text{-}S_{C5}\right),\ v_\beta = \frac{V_{dc}}{3}\left[\sqrt{3}\left(2S_{C1}\text{-}S_{C5}\right)\right] \quad (3)$$

The sensed stator currents (i_{gena} and i_{genb}) are expressed in αβ0 frame (i_α and i_β) as,

$$i_\alpha = i_{gena},\ i_\beta = \frac{1}{\sqrt{3}}\left(i_{gena} + 2i_{genb}\right) \quad (4)$$

The stator fluxes (ψ_α and ψ_β) are estimated as,

$$\psi_\alpha = \int e_\alpha dt = \int \left(v_\alpha + R_s i_\alpha\right)dt,\ \psi_\beta = \int e_\beta dt = \int \left(v_\beta + R_s i_\beta\right)dt \quad (5)$$

where, e_α and e_β are the BEMFs and R_s is the stator resistance.

The generator speed (ω_g) and position (θ_g) are estimated as,

$$\omega_g = \frac{\left(\psi_\alpha \frac{d}{dt}\psi_\beta - \psi_\beta \frac{d}{dt}\psi_\alpha\right)}{p\sqrt{\psi_\alpha^2 + \psi_\beta^2}},\ \theta_g = \tan^{-1}\left(\frac{\psi_\beta}{\psi_\alpha}\right) \quad (6)$$

where p is the PMSG pole pairs.

2) Speed Control of PMSG

The speed of the PMSG is regulated using the FOC method. The ω_{gref} generated from the hill climbing MPPT technique is compared with the ω_g and inputted to the speed PI controller for the generation of the reference quadrature axis current (I_{qref}) as,

$$I_{qref} = \left(K_{p\omega} + \frac{K_{i\omega}}{s}\right)\left(\omega_{gref} - \omega_g\right) \quad (7)$$

where, $K_{p\omega}$ and $K_{i\omega}$ are the speed controller gains.

As the PMSG does not require external excitation due to presence of permanent magnets on the rotor, the reference direct axis current (I_{dref}) is set as zero.

These reference currents are converted from dq0 to abc reference frame and compared with the stator currents for generating the switching signals (S_{C1}-S_{C6}) using the hysteresis controller.

C. Control of DC Link Voltage and BDC

The V_{dc} is controlled in such a way that the optimum power is harnessed from the solar PV array. When the grid is available, the V_{dc} is controlled by the GSC and the output of the V_{dc} controller is taken as weight of the DC loss component (W_{loss}) whereas when the grid is unavailable, the V_{dc} is controlled by the BDC and the controller output is taken as reference battery current (I_{bref}). For controlling the V_{dc}, the V_{pvref} from the hill climbing MPPT technique is compared with the V_{dc} and the error is fed to the V_{dc} PI controller. The controller output is given as,

$$\left(K_{pdc} + \frac{K_{idc}}{s}\right)\left(V_{pvref} - V_{dc}\right) = \begin{Bmatrix} W_{loss}; \text{ grid is available} \\ I_{bref}\ ; \text{ grid is unavailable} \end{Bmatrix} \quad (8)$$

where, K_{pdc} and K_{idc} are the V_{dc} controller gains.

During grid unavailability, the I_{bref} is generated from the V_{dc} controller whereas when the grid is available, the I_{bref} is set externally according to the required energy demand. Once the I_{bref} is generated, it is compared with the battery current (I_{bat}) and the battery current error (I_{berr}) is fed to the hysteresis controller for generating the switching signals (S_{bu} and S_{bl}) for the upper and lower switches of the BDC as shown in Fig. 3.

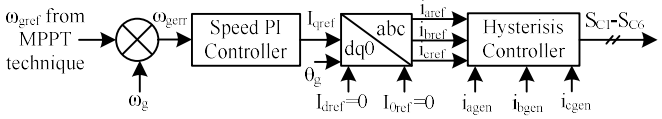

Fig. 2. Control of WEGS

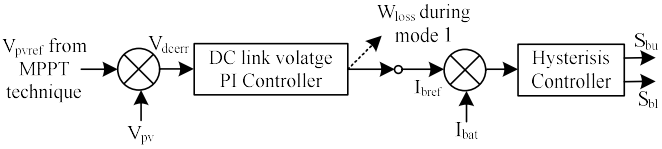

Fig. 3. Control of DC link voltage and BDC

D. Control of GSC

Fig. 4 demonstrates the control strategy for the GSC. The control of GSC comprises the estimation of the load component, estimation of the net weight component, generation of reference grid current and generation of the switching signals for GSC. The FA-DSOGI is used here for estimating the fundamental load component.

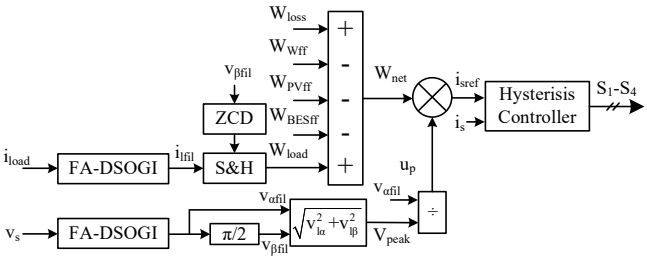

Fig. 4. Control of GSC

1) Estimation of Load Component

The load current active power component is estimated using the FA-DSOGI control structure. The structure of the frequency adaptive damped SOGI (FA-DSOGI) is shown in Fig. 5. The proposed control structure estimates the filtered fundamental load components (i_{lfil}) and rejects the harmonics from the distorted grid current. The transfer function for the FA-DSOGI is given as,

$$TF_{FA\text{-}DSOGI} = \frac{\omega_{est}\left(s+\rho\right)}{\left(s+\rho\right)^2 + \omega_{est}^2} \quad (9)$$

The state space equations for FA-DSOGI are expressed as,

$$\frac{di_{l5}}{dt} = k_2 \omega_{est} i_{l1} \quad (10)$$

$$\frac{di_{l3}}{dt} = -\rho i_{l3} + \omega_{est} i_{lfil} \quad (11)$$

$$\frac{di_{lfil}}{dt} = -\omega_{est} i_{l3} - \rho i_{lfil} + k_1 \omega_{est} i_{l1} \quad (12)$$

where, ω_{est} is the estimated grid frequency in rad/sec and ρ is the damping factor. i_{l1}, i_{l2}, i_{l3}, i_{l4}, i_{l5} and i_{l6} are the extracted load components.

The load component (W_{load}) is estimated by sampling and holding the i_{lfil} at every instant when the filtered quadrature component of the grid voltage ($v_{\beta fil}$) crosses zero value.

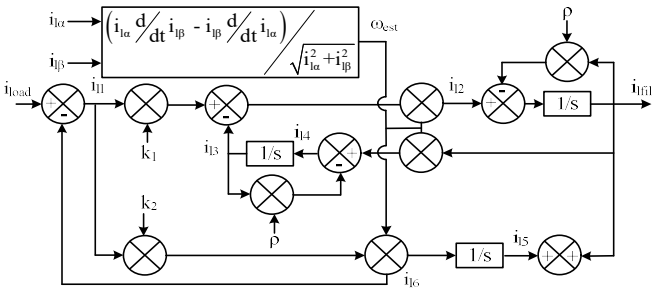

Fig. 5. Control structure of FA-DSOGI

2) Estimation of Net Component

The feed-forward terms are employed for improving the dynamic performance of the presented system. The estimation of the net component comprises the DC loss component (W_{loss}), wind feed-forward component (W_{Wff}), PV feed-forward term (W_{PVff}), battery feed-forward term (W_{BESff}) and load component (W_L).

The W_{loss} is estimated as the output of the V_{dc} controller. The W_{Wff}, W_{PVff} and W_{BESff} are given as,

$$W_{Wff} = \frac{P_W}{V_t},\ W_{PVff} = \frac{P_{PV}}{V_t},\ W_{BESff} = \frac{P_{BES}}{V_t} \tag{13}$$

where, P_W, P_{PV} and P_{BES} are the power output from WEGS, solar PV array and BES respectively. V_t is the terminal voltage at PCC.

The net component (W_{net}) is calculated as,

$$W_{net} = W_{loss} - W_{Wff} - W_{PVff} - W_{BATff} + W_{load} \tag{14}$$

3) Switching Pulse Generation

For the generation of switching pulses, the reference grid current (i_{sref}) is evaluated as,

$$u_p = \frac{v_{\alpha fil}}{V_{peak}},\ i_{sref} = u_p * W_{net} \tag{15}$$

where, u_p is the in-phase unit template, $v_{\alpha fil}$ is the filtered in-phase component of the grid voltage and V_{peak} is the peak value of the grid voltage.

This i_{sref} is compared with the sensed grid current (i_s) using the hysteresis controller for generating the switching pulses (S_1-S_4) for the GSC.

III. Performance of FA-DSOGI

The performance of FA-DSOGI is realized under distorted load current and frequency change. It can be visualized from Fig. 6(a) and Fig. 6(b) that the FA-DSOGI effectively extracts the fundamental load current and tracks the variation in frequency respectively.

IV. Results and Discussion

The performance of the presented wind-solar-BES based AC microgrid utilizing the FA-DSOGI based control structure is validated experimentally using the developed laboratory prototype. A dSpace 1202 is utilized for implementing the control of the presented system. The ratings of the system parameters are enumerated in Appendix.

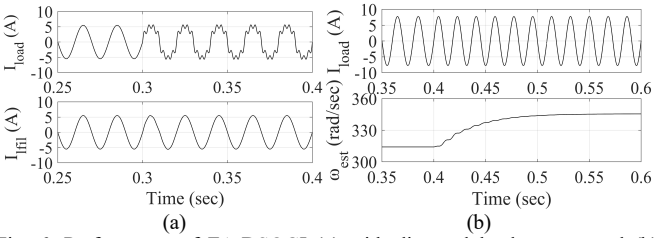

Fig. 6. Performance of FA-DSOGI (a) with distorted load current and (b) during frequency change

A. Steady State Performance

The steady-state behavior of the presented system is shown in Fig. 7. It can be anticipated from Fig. 7(a) that owing to the implementation of FOC, the stator currents of the PMSG are sinusoidal. With the tracking efficiency above 99%, an excellent MPPT performance of the solar PV array is exhibited in Fig. 7(b). It can be visualized from Fig. 7(c) that even when the load current is distorted, the grid current is sinusoidal. This has been achieved through the implementation of the FA-DSOGI based control structure. An effective BES charging through BDC is depicted in Fig. 7 (d).

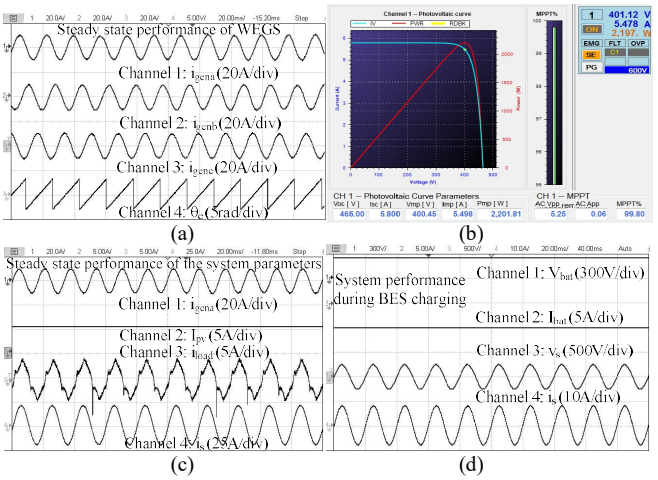

Fig. 7. Steady-state performance of the presented system

B. Dynamic Performance

The dynamic performance for the wind speed (v_w) change is depicted in Fig. 8 (a). As the v_w is changed from 12 m/s to 8.4 m/s, the ω_g also changes such that the peak power is harnessed from the WEGS. The WEGS power (P_g) decreases for reduction in v_w. The W_{Wff} also follows this variation. Fig. 8(b) shows the variation in the weight component with the variation in v_w. Since the solar PV generation and local load are constant, no variation in W_{PVff} and W_{load} is realized. However the W_{net} and consequently the injected grid power decreases with reduction in v_w and vice-versa.

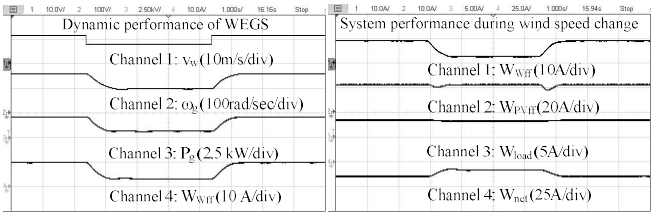

Fig. 8. Dynamic performance under wind speed change

The dynamic performance of the system for the solar insolation variation is depicted in Fig. 9. It can be anticipated from Fig. 9(a) that the reduction in insolation from 1000 W/m^2 to 500 W/m^2 reduces the I_{pv} to around half of the previous value. A marginal drop in V_{pv} is observed for insolation change, however, the P_{pv} reduces significantly. The W_{PVff} also follows the change, however the W_{Wff} and W_{load} remain unperturbed. With the reduction in PV power, the power input to the grid also reduces and results in the reduction of W_{net}. Various system parameters are restored to the previous values once the solar insolation is restored to 1000 W/m^2.

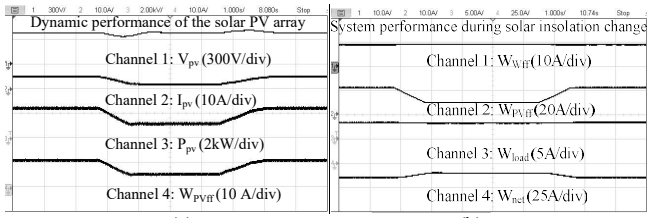

(a) (b)

Fig. 9. Dynamic performance under insolation change

C. PQ Performance

The PQ performance of the presented system is shown in Fig. 10. It can be realized from Figs. 10 (a-f) that a non-linear load with a current THD of 13.3 % is connected to the grid. However, the grid current THD is 2.4 %, which is within the limits stated under the IEEE-519 standard. The PQ performance when both the sources i.e. wind and solar are feeding the grid and load is shown in Figs. 10 (g-i). A grid current of 14.26 A with THD of 3.2 % is fed to the grid under this scenario.

The PQ performance when BES is feeding the grid and vice-versa is shown in Figs. 10(j-o). The grid draws a power of 1.3 kW at a THD of 4.9 % while charging the BES whereas when BES is feeding the grid, a power of 1.03 kW at THD of 4.2 % is fed to the grid. It can be realized that under all scenarios, the grid current THD remains within the limits stated in the IEEE-519 standard and, therefore, shows the efficacy of the presented control structure.

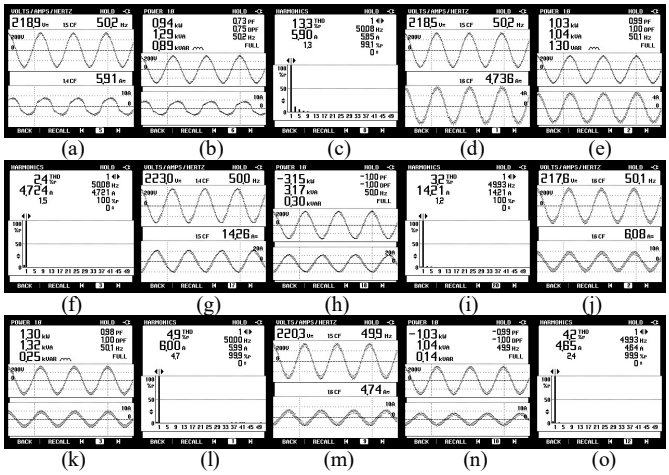

(a) (b) (c) (d) (e)

(f) (g) (h) (i) (j)

(k) (l) (m) (n) (o)

Fig. 10. PQ performance

V. Conclusion

Experimental results for the wind-solar-BES based AC microgrid under various operating scenarios validate the effectiveness of the FA-DSOGI based control structure. The steady-state and dynamic performances are found to be satisfactory. The presented FA-DSOGI has successfully extracted the fundamental load component and alleviated the noise signal. The hill climbing MPPT technique has effectively extracted the optimum power from the WEGS and solar PV array. The FOC for the speed control of the PMSG and BEMF technique based rotor speed and position estimation has been well implemented. By the virtue of the FA-DSOGI, the presented system provides an improved PQ performance and the grid current THD remains within the limits stated under IEEE-519 standard.

Acknowledgement

This work was supported by the Agency for Science, Technology and Research (A*STAR) through its Singapore-Germany Academic-Industry (2+2) International Collaboration under Grant A1990b0060.

Appendix

PMSG Parameters: 3hp, 230 V, n = 4, R_s= 1.5 Ω, L_s= 3.5 mH
PV Array Parameters: V_{oc}= 465 V, I_{sc}=4.8 A, V_{mp}= 400.45 V, I_{mp}=5.498 A, P_{mp}=2201.81 W
FA-DSOGI Parameters: k_1=1.4, k_2=1.2, ρ=0.42
Ripple Filter: R_f = 5Ω, C_f = 10 μF

References

[1] Z. Yang, J. Hu, X. Ai, J. Wu and G. Yang, "Transactive Energy Supported Economic Operation for Multi-Energy Complementary Microgrids," *IEEE Trans. Smart Grid*. [Early Access]

[2] W. Yan, L. Cheng, S. Yan, W. Gao and D. W. Gao, "Enabling and Evaluation of Inertial Control for PMSG-WTG Using Synchronverter With Multiple Virtual Rotating Masses in Microgrid," *IEEE Trans. Sust. Energy*, vol. 11, no. 2, pp. 1078-1088, April 2020.

[3] M. Abdelrahem, C. M. Hackl, R. Kennel and J. Rodríguez, "Computationally Efficient Finite-Position-Set-Phase-Locked Loop for Sensorless Control of PMSGs in Wind Turbine Applications," *IEEE Trans. Pow. Elect.*, vol. 36, no. 3, pp. 3007-3016, March 2021.

[4] W. Zhu, L. Shang, P. Li and H. Guo, "Modified hill climbing MPPT algorithm with reduced steady-state oscillation and improved tracking efficiency," *The J. Engg.*, vol. 2018, no. 17, pp. 1878-1883, Nov 2018.

[5] J. Rocabert, R. Capó-Misut, R. S. Muñoz-Aguilar, J. I. Candela and P. Rodriguez, "Control of Energy Storage System Integrating Electrochemical Batteries and Supercapacitors for Grid-Connected Applications," *IEEE Trans. Ind. Appl.*, vol. 55, no. 2, pp. 1853-1862, March-April 2019.

[6] "*IEEE Recommended Practice and Requirements for Harmonic Control in Electric Power Systems*," IEEE Std 519-2014 (Revision of IEEE Std 519-1992), vol., no., pp.1-29, 11 June 2014.

[7] C. Zhang, S. Yu, K. Jiang, X. Ge and J. Ma, "A Fast Instantaneous Power Calculation Algorithm for Single-Phase Rectifiers Based on Arbitrary Phase-Delay Method," *IEEE Trans. Ind. Appl.*, vol. 55, no. 4, pp. 3935-3945, July-Aug. 2019.

[8] S. Gude and C. Chu, "Dynamic Performance Improvement of Multiple Delayed Signal Cancelation Filters Based Three-Phase Enhanced-PLL," *IEEE Trans. Ind. Appl.*, vol. 54, no. 5, pp. 5293-5305, Sept.-Oct. 2018.

[9] A. Parida and B. Subudhi, "Modified leaky LMS-based control strategy for reliable operation of single-stage three-phase grid-tied PV system," *IET Renew. Pow. Gen.*, vol. 14, no. 9, pp. 1453-1462, July 2020.

[10] J. Matas, H. Martín, J. de la Hoz, A. Abusorrah, Y. A. Al-Turki and M. Al-Hindawi, "A Family of Gradient Descent Grid Frequency Estimators for the SOGI Filter," *IEEE Trans. Pow. Elect.*, vol. 33, no. 7, pp. 5796-5810, July 2018.

[11] S. Golestan, J. M. Guerrero, F. Musavi and J. C. Vasquez, "Single-Phase Frequency-Locked Loops: A Comprehensive Review," *IEEE Trans. Pow. Elect.*, vol. 34, no. 12, pp. 11791-11812, Dec. 2019.

[12] C. M. Nirmal Mukundan, P. Jayaprakash, U. Subramaniam and D. J. Almakhles, "Binary Hybrid Multilevel Inverter-Based Grid Integrated Solar Energy Conversion System With Damped SOGI Control," *IEEE Access*, vol. 8, pp. 37214-37228, 2020.